Solvation, Water Permeation, and Ionic Selectivity of a Putative Model for the Pore Region of the Voltage-Gated Sodium Channel

Chandralekha Singh,* R. Sankararamakrishnan,# Shankar Subramaniam,# and Eric Jakobsson#
*Department of Materials Science and Engineering and #Department of Molecular and Integrative Physiology, Center for Biophysics and Computational Biology, National Center for Supercomputing Applications, Beckman Institute for Advanced Science and Technology, University of Illinois, Urbana, Illinois 61801 USA

ABSTRACT This paper describes a molecular dynamics and molecular mechanics study of the solvation and selectivity of the narrow pore and vestibule region of a model-built structure for the voltage-gated sodium channel. The particular structure used was one proposed by Guy and Durell. However, many of the features we saw would likely be shared with other possible models for this channel, such as the one proposed by Lipkind and Fozzard. It was found that the water mobility was reduced in the channel and the water orientations were significantly ordered by the channel environment. Water mobility depended on protein mobility; in a computer experiment in which the protein was artificially frozen, channel water at 300°K was immobilized. Water motions were defined in significant part by a series of discrete moves from one pattern of hydrogen bonding with particular amino acids to another. However, there are so many different hydrogen bonding patterns that a description of the motion in terms of transitions among a small number of discrete states is not appropriate. In the model whose solvation we explored, several charged residues seem to play a particularly significant role in determining solvation and water motions. Based on energy minimization studies, the structure clearly shows selectivity for univalent cations over anions.

INTRODUCTION

In considering structure-function relationships in soluble proteins, the problem often starts with a well-defined structure. For membrane proteins, very few high-resolution structures are available. The recent overview of the state of membrane protein structure determination by a variety of methods is given by White (1994). Ion channels are unusual proteins in that extremely precise functional data of the behavior of single protein molecules is available (Hille, 1992). Perhaps because of this there is a relatively long and somewhat successful history of postulating ion channel structure in the absence of complete structural data. On the basis of very incomplete solution NMR data, Urry (1971) postulated that the ion channel formed by the antibiotic gramicidin was a dimer composed of two head-to-head β-bonded helices. This structural motif was conclusively confirmed much later by solid-state NMR (Arseniev et al., 1985; Nicholson and Cross, 1989). Other biologically important ion channels are too large for complete structural determination by this method. However, model-building based on general principles of protein structure in tandem with molecular biology and electrophysiology experimentation have yielded insights into the probable structure of the voltage-gated channels. For example, Guy and Seetharamulu (1986) postulated that the narrow part of the pore in voltage-gated sodium channels consisted of the linker (called the P region) between two transmembrane-spanning regions, designated as S5 and S6. Numerous mutagenesis/electrophysiology studies in the intervening years have confirmed this hypothesis for sodium-, calcium-, and potassium-selective channels (Guy and Durell, 1995). As the mutagenesis/electrophysiology experiments have continued, they have constrained the possible models for the pore and selectivity regions more rigorously. Detailed models for the sodium channel pore regions have been put forward by two groups (Lipkind and Fozzard, 1994; Guy and Durell, 1995). In the case of the sodium channel, which is the subject of this paper, major constraints on models of the P region are the identity of the residues that are critical for sodium selectivity and for the binding of the toxins that are specific for voltage-dependent sodium channels, tetrodotoxin (TTX) and saxitoxin (STX). Fig. 1 *a* shows the sequence of the segment of the channel model whose behavior has been considered in this study. (In the discussion that follows, we use the Guy and Durell (1995) notation for numbering residues in the P region and correlate that with our numbering as shown in Fig. 1 *a*.) Residues that seem to be critical for sodium selectivity include the 14p residue in each repeat, which would be the residues numbered 19, 53, 85, and 117 in our numbering scheme shown in Fig. 1 *a*. The evidence for this is from experiments in which mutations at the 14p location can make sodium channels adopt calcium selectivity (Heinemann et al., 1992) or calcium channels adopt sodium selectivity (Kim et al., 1993; Mikala et al., 1994; Yang et al., 1993). These residues plus those in the 17p location (22, 56, 88, and 110 in our numbering scheme) are critical for the binding of STX and TTX, blockers that are specific for sodium channels (Terlau et al., 1991). Functionally it also should be noted from radioactive

Received for publication 27 September 1995 and in final form 30 July 1996.

Address reprint requests to Dr. Eric Jakobsson, NCSA, 4039 Beckman Institute, University of Illinois, 405 North Matthews Ave., Urbana, IL 61801. Tel.: 217-244-2896; Fax: 217-244-2909; E-mail: jake@ncsa.uiuc.edu.

Dr. Singh's present address is Physics Department, University of Pittsburgh, Pittsburgh, PA 15260.

0006-3495/96/11/2276/13 $2.00

A

SEGMENT I: SYDTFSWAFLALFRLMTQDYWENLFQLTLRAAAG
RESD. NO. : 1 34

SEGMENT II: HMNDFFHSFLIVFRILCGEWIETMWDCMEVAG
RESD. NO. : 35 66

SEGMENT III: NYDNVGLGYLSLLQVATFKGWMDIMYAAVDSR
RESD. NO. : 67 98

SEGMENT IV: NFETFGNSIICLFEITTSAGWDGLLNPILNSG
RESD. NO. : 99 130

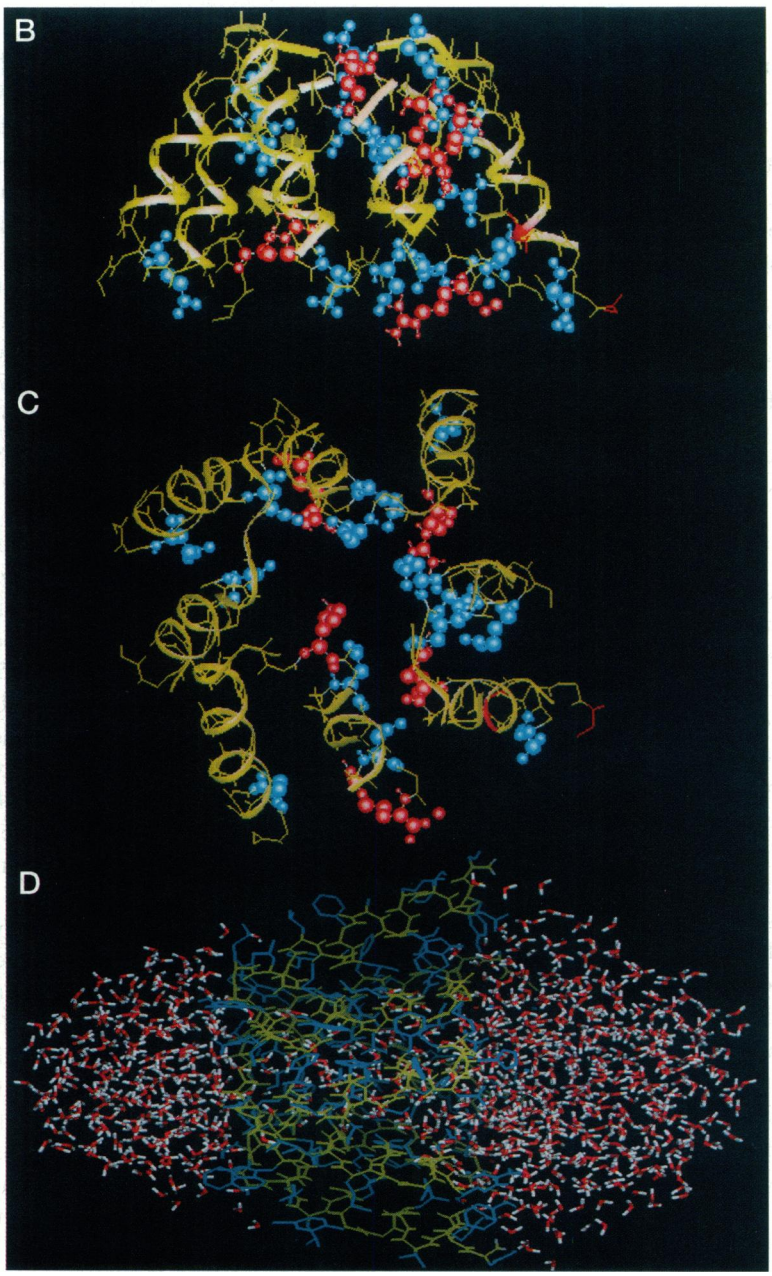

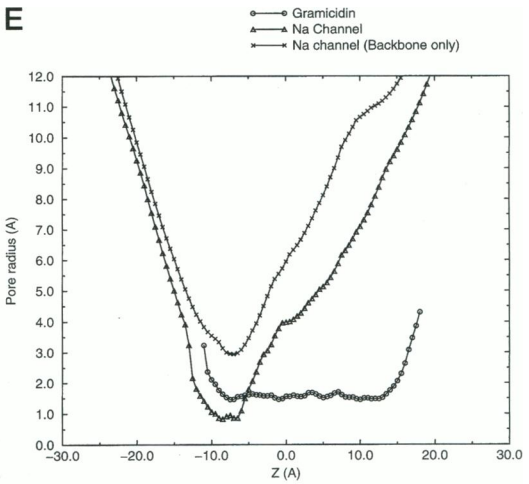

FIGURE 1 (*a*) Sequence of the modeled segment of the voltage-gated sodium channel. The residues forming the turn whose structure is critical for selectivity and toxin binding are 19 through 22 in the first repeat, 53 through 56 in the second repeat, 85 through 88 in the third repeat, and 107 through 110 in the fourth repeat. (*b*) Visualization of the modeled segment from a side view in the plane of the membrane, including the backbone plus the side chains of the charged residues (*red*, positive; *blue*, negative). (*c*) Visualization of the modeled segment viewed from the channel axis, including the backbone plus the side chains of the charged residues (red, positive; blue, negative). (*d*) The solvated channel structure showing the water hemispheres at each end of the channel, as described in the text. (*e*) The channel radius as a function of position along the channel axis, as measured by the method of Smart et al. (1993), for the sodium channel including side chains (△), for the sodium channel without side chains (*crosses*), and for purposes of comparison, the gramicidin channel (○).

tracer flux-ratio experiments that the voltage-gated sodium channel probably has only a short narrow region, because fluxes in one direction through the channel do not interfere significantly with fluxes in the opposite direction at physiological concentrations. This is in contrast to voltage-gated potassium channels, which do show interference between unidirectional fluxes, thus suggesting a longer narrow region. (For a review of the tracer flux literature, see Hille, 1992.) It may be significant in this regard that potassium channel P sequences have more residues than do sodium channel P sequences.)

From the above considerations it is strongly suggested that the appropriate model for the sodium channel includes a hairpin turn involving residues 14p through 17p (19–22, 53–56, 85–88, and 117–110 in our numbering system) that defines the selectivity filter and the TTX/STX binding site. The remainder of the P region would form a vestibule wide enough for ions to pass each other, and of course should be lined with hydrophilic groups. There are several ways to construct a model that would fulfill these requirements. Guy and Durell (1995) have proposed a model with a helix-turn-helix motif, whereas Lipkind and Fozzard (1994) proposed a β hairpin.

In this paper we present an initial study of the solvation of one of the Guy and Durell models. It follows the logic of our earlier explorations of the gramicidin channel (Chiu et al., 1989, 1991, 1992, 1993). That logic begins with the premise that a key element of channel function is moving an ion from the aqueous solvation environment to the channel solvation environment. Thus a reasonable first step in understanding ion channel function is to understand the solvation of the pore region of the channel, the topic of this paper. In the gramicidin channel the long narrow pore dimensions mandate that water molecules move through the channel in single file. This will not be true for the sodium channel model presented here because the channel, even at its narrowest part, is wide enough for waters to move through side by side. This feature would probably be true for any reasonable model of the sodium channel, based on the size of ions that can permeate the channel (Hille, 1992). In the gramicidin channel it was found that the mobility of water in the channel was substantially smaller than in bulk. At any particular time there is a strong tendency in the gramicidin channel for the water dipoles to be oriented in the same direction relative to the channel axis. However, there is no net preference averaged over time for the dipoles to be oriented toward one or the other end of the channel, because of the symmetry of the channel structure. We will explore the ways in which the mobility and orientional preferences of the voltage-gated sodium channel model are similar to, and different from, the gramicidin channel.

In addition to the solvation, we show an initial calculation of selectivity in the channel, based on the relative energies of the system with ions of different species at the narrowest portion of the permeation pathway.

METHODS

Model structure

Fig. 1 *a* shows the sequence of the p region of the four sodium channel subunits that are included in the model system simulated in this paper. The sodium channel is modeled as a heteromeric tetramer, with each monomer containing between 32 and 34 residues. Fig. 1 *b* shows the channel structure from a side view (within the membrane plane). Fig. 1 *c* shows the same structure, looking down the channel axis. In Fig. 1 *b* shows the channel backbone and the charged residues (red, positive; blue, negative). The length of the channel as characterized by the distance between the farthest backbone atoms on the cytoplasmic and the extracellular sides is approximately 22 Å. This structure (from Guy and Durell, 1995) is consistent with the data cited above suggesting which residues are at the narrowest part of the channel, but is not claimed to be unique. Other arrangements of the heteromer might also be consistent with these data. The four helix-helix segments have hydrophilic residue side chains lining the pore. The model consists of 130 residues, which include 19 charged, 34 polar, and 77 nonpolar (hydrophobic) residues. Most of the hydrophobic residues are outside the channel in contact with the rest of the protein. Within a united atom approach for methyl, methylene, and methine groups, the total number of atoms involved in the model is 1270. Hydrophilic residues point into the channel, where they are in a position to play a major role in steering and propelling the waters through the channel. These include 85 LYS (85 refers to the residue number in our numbering scheme of Fig. 1 *a*), 89 ASP, 48 ARG, 56 GLU, 53 GLU, 14 ARG, 19 ASP, 23 ASN, 22GLU, 119ASN, and 128. 85 LYS is the only LYS in the model structure and is located in the narrowest region of the pore. (In the terminology of Guy and Durell (1995), this is the 14p residue in repeat III.) In Fig. 1 *c* the LYS 85 in the narrowest part of the channel is shown with particular clarity. It seems odd that a LYS should be in the narrowest region of a cation-selective pore, but the combined electrophysiology/site-directed mutagenesis studies showing which residues have critical effects on sodium/calcium selectivity seem to lead unavoidably to this arrangement. In addition to the above-cited studies on 14 p mutations (Heinemann et al., 1992; Kim et al., 1993; Mikala et al., 1994; Yang et al., 1993), more recent data (Favre et al., 1996) further clarify the role of the LYS in this position. Favre et al. showed that if a residue other than LYS or ARG is placed in this position, the channel is selective for calcium over sodium. The ARG mutation in this position retains monovalent over divalent cation selectivity but destroys sodium over potassium selectivity. Thus the LYS 85 seems to be a critical determinant of sodium channel identity. Its positive charge is apparently critical for making the channel selective for sodium over calcium, and its size and conformation are apparently critical for making the channel selective for sodium over potassium.

To emulate the electrolyte environment of the channel, the model structure is initially solvated to a distance of 2.3 Å. Moreover, hemispherical water caps with radii of 20 Å and 17 Å are introduced at the wide (extracellular) and narrow (intracellular) pore ends, respectively, to emulate a bulk-like solvation environment. Fig. 1 *d* is a snapshot of the solvated sodium channel structure. The complete solvated structure consists of 933 water molecules, of which approximately 43–45 are inside the channel on average at all times. The water model is SPC (Hermans et al., 1984). This model was originally designed to be compatible with the GROMOS protein force fields.

Another way of visualizing the channel structure is to show the pore radius as a function of position along the channel axis. This can be done by the method of Smart et al. (1993), using the program HOLE. This method sizes a pore by finding, at each position along the channel axis, the smallest sphere centered at that point that will fit in the channel. Fig. 1 *e* shows the channel sizing from this method, for the energy-minimized sodium channel model including side chains (triangles) and the sodium channel omitting the side chains (crosses). It is seen that the radius for the channel at the narrowest part, including side chains, is approximately the size of the bare sodium ion. For comparison, the same analysis was done for a gramicidin channel (circles). The gramicidin channel in this case was a time-averaged structure from 10 ps of a molecular dynamics simulation of the channel embedded in lipid and containing water (Chiu et al., 1996a).

For the energetic calculation of Table 1 (interaction energy between an ion and channel residues when an ion is in the narrowest part of the channel), the ionic van der Waals parameters for sodium and potassium are as determined by Aqvist (1990). The criterion is that these parameters give appropriate solvation energies in SPC water. The chloride ion parameters are default parameters in the GROMOS package.

TABLE 1 Electrostatic interaction energies (kJ/mol) between the ion under study and polar residues in the narrow region, the whole protein, and solvent molecules

Residue	Na^+	K^+	Cl^-
Asp 19	−220.0	−206.0	+232.8
Glu 53	−215.1	−204.1	+201.0
Glu 56	−230.6	−232.9	+200.9
Lys 85	+434.1	+391.2	−420.4
Asp 89	−223.3	−236.4	+205.3
Asp 120	−192.8	−192.6	+214.5
Protein	−639.9	−675.1	+612.8
Water	−228.5	−153.1	−82.1

Energies are from an energy-minimized configuration with the ion at the most narrow part of the channel.

Simulation methodology

The solvation data in this paper were from a 520-ps molecular dynamics simulation at 300°K. Simulations were performed using the leapfrog algorithm with GROMOS force fields. The SHAKE algorithm was used to keep the bond distances within a given tolerance. The long-range nonbonded Coulomb interaction atom pair list was updated every 50 steps. The cutoff radius for calculating such pair interactions was chosen to be 1.2 nm. The cutoff was charge group-based, using the standard GROMOS conventions for defining charge groups. In our experience, this cutoff distance of 1.2 nm is appropriate for a well-solvated system such as this. It would not be large enough for a membrane simulation where much of the system is low-dielectric hydrocarbon (Chiu et al., 1996a). The time step for MD simulations was 2 fs.

Because the computed macromolecular system was only a protein channel fragment without either the rest of the protein or the surrounding lipid included, artificial restraints were used to stabilize the system. These restraints are essentially the same as those used by our laboratory in earlier simulations of the gramidicidin channel (Chiu et al., 1989, 1991). Below we review this strategy briefly and describe its implementation for the sodium channel pore region that is the subject of this paper. Under these restraints the new position of an atom is modified by applying a change that pulls it toward a reference position with a specified relaxation time, according to the expression $dr/dt = (r_0 - r)/\tau_r$. In this expression τ_r is the relaxation time for each atomic position to relax toward its specified reference position. The initial reference positions were chosen to be the atom positions in the starting structure. If the relaxation time is large, the restraining tendency toward the reference position is small. This restraint changes only the position of the atom directly. The ultimate effect of this sort of restraint is to maintain the secondary structure of the protein and the general orientation of secondary structural units close to the reference structure, but to leave local motions largely unmodified. In the simulations described in this paper we impose a 40-ps restraint on the protein backbone while allowing the side chains to move freely. This weak restraint does not significantly affect the local motion of the backbone, but prevents large global motion so that the channel structure remains intact at all times. To prevent the waters from wandering off the hemispherical caps, a 40-ps restraint was applied to waters outside the specified cap dimensions to pull them toward the center of the hemispherical cap.

To keep the temperature constant we coupled the system to a heat bath (Berendsen et al., 1984), with independent coupling of the water and the protein. The velocity of all atoms was rescaled at each step to keep the temperature of the system constant. Once equilibration was achieved, the velocity rescaling factors were near unity, implying negligible exchange of heat with the bath. The heat bath coupling was maintained throughout the molecular dynamics simulation. There are two reasons for keeping the coupling on.

One is that for a system with a large protein or protein fragment, even if the system is well equilibrated, there may be conformational shifts during the simulation that cause significant shifts in the potential energy. If the simulation is done at constant energy (i.e., without continuous coupling to the temperature bath), such potential energy shifts will cause appreciable changes in the temperature. Thus the system was continuously coupled to the heat bath to ensure maintenance of constant temperature. A further reason for maintaining coupling is that the soft 40-ps restraints as described above are not conservative. Thus the restraints would give rise to a drift in the temperature, unless coupling to a temperature bath were maintained during the simulation. Based on analysis of simulations of pure water, continuous coupling to the heat bath does not introduce any artifacts into the water dynamics.

To improve the structure locally and remove bad local contacts, we carried out an energy minimization on the initial model structure before performing the MD simulations. Only a few hundred steps were required to attain the local potential energy minima. The system was then heated to 300°K using MD simulations with reassignment of velocity from a Maxwell-Boltzman distribution every 0.2 ps. The MD with velocity reassignment was continued for a total of 100 ps. This was followed with another 100 ps of continuous MD without velocity reassignment to ensure proper equilibration before the data collection began. Because the starting structure was not the equilibrium structure, the reference position toward which the backbone atoms are restrained was constantly updated during the heating and equilibration process. The new reference position is taken to be the average of the last five positions. After the system was equilibrated, the reference positions for the restraint were kept constant for the duration of the simulation. The major part of the simulation was a continuous MD at 300°K for 520 ps.

In the energetic calculation for Table 1, the starting point was the well-solvated and equilibrated sodium channel P region. For each of three ionic species the ion was placed on the channel axis, at the narrowest point of the channel. The energy was minimized by the conjugate gradient method, to a tolerance of 0.001 kJ/mol.

Analysis

We analyze the dynamic behavior of the model in two basic ways. One mode of analysis is based on the average structural and time-dependent properties. A second mode of analysis is necessitated by the fact that critical events occur in the narrow part of the channel that involve just one or a few water molecules and one or a few amino acids at a time. Thus it is important to look at trajectories and interactions involving individual water molecules.

With respect to average properties, a useful measure of mobility is the mean square deviation (MSD) correlation. The mean square deviation is the mean square distance traveled in a time, i.e.,

$$\mathrm{MSD}(\tau) = \int_{t=0}^{t=t_{max}-\tau} \mathrm{d}t[x(t+\tau) - x(t)]^2.$$

The mean square deviation in position and the total number of dihedral transitions associated with various residues are monitored. We also calculate the pair correlation function $g_{xy}(r)$, which is a measure of the local packing. It is the probability of finding an atom y at a distance r from an atom x. The integral of this quantity over a spherical shell of radius r and $r + \mathrm{d}r$ is useful for calculating the coordination number, because it yields the total number of y at a distance r from x.

With respect to individual water motions, we analyze the trajectories and dipole moment orientations of individual waters inside the channel throughout the simulation and the waters that are close to the narrow pore region for a significant fraction of time. Some cap waters are also analyzed to distinguish them from the channel waters. The correlation between the motion of waters near the narrow pore and the side-chain residues is analyzed in terms of the formation and disruption of hydrogen bonds between them as a function of time. We also calculate the mean square deviation (MSD) of the channel and cap waters, and from the short and long time slopes of the MSD curve deduce the hydrodynamic and effective diffusion constants, respectively. The trajectory, dipole moment orientation, and MSD of the center of mass of the channel waters are also studied to assess any collective motion of water in the channel.

RESULTS

To ensure proper equilibration and the absence of any systematic drift, we plot the potential energy as a function of time in Fig. 2. The initial heating to 300°K is attained rather quickly in 10–20 ps. In the first 100 ps, when the velocity

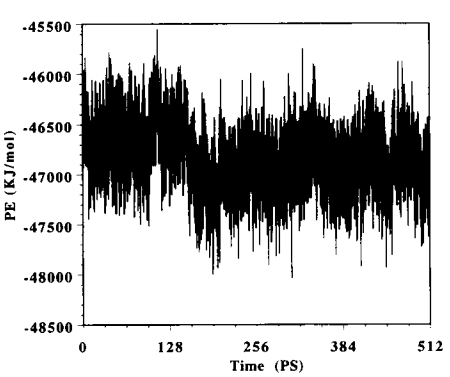

FIGURE 2 Total potential energy as a function of time during the continuous molecular dynamics simulation at 300°K. The system was considered to be equilibrated during the time that the potential energy was essentially unchanging with time.

is reassigned every 0.2 ps from a Maxwell-Boltzmann distribution, the total and potential energies simply fluctuate about some average values. After 100 ps, when simulations are performed without the velocity reassignments, there appears to be an initial increase in the total energy. Gradually the total energy decreases and the system attains equilibrium. After 200 ps the total energy fluctuates about a value that is a few hundred kilojoules lower than the average total energy during the initial heating cycle. Because we hold the temperature fixed at 300°K, the kinetic energy of the system is a constant. After equilibration the root mean square fluctuations in both the potential and total energies are less than 1%. All analysis shown in this paper begins after the initial 200 ps equilibration.

The radius of gyration was also monitored as a function of time. During the heating and equilibration period there was a small but gradual increase in the radius of gyration. Once the system equilibrated, the radius of gyration simply fluctuated about an average value.

In Fig. 3 we plot the density-normalized water-water pair correlation functions, $g_{OW\text{-}OW}(r)$, for bulk SPC water and for waters inside the channel and in the hemispherical caps. (The bulk computation was done by Dr. See-Wing Chiu.) The pair correlation is the probability of finding an atom y at a distance r from an atom x. In this case we normalize the pair correlation function relative to the density of bulk water, so that the bulk water curve is asymptotic to unity at large values. Apart from the primary shell structure, the pair correlation function of the cap water also shows well-defined secondary (second and third) solvation shells, reflecting the packing of cap waters with each other. It is seen that the positioning and width of the peaks representing the solvation shells are essentially identical to the corresponding features of the radial distribution function for bulk water. This suggests that the local water structure out to the third solvation shell is essentially the same for the cap water in this simulation, as it is in bulk water. Over the long range the function for bulk water is asymptotic to 1 (bulk density),

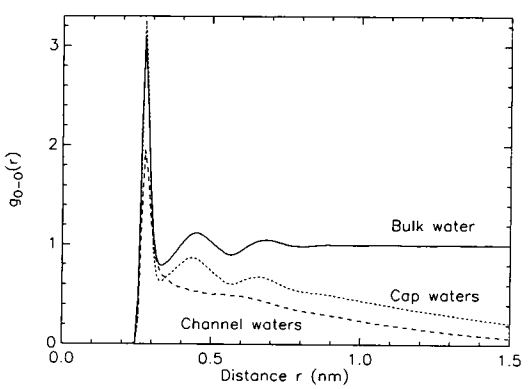

FIGURE 3 Water-water pair correlation function ($g_{O\text{-}O}$) for water molecules inside the channel (*long dashes*), in the hemispherical caps (*short dashes*), and in bulk water (*solid line*). It is seen that there are well-defined hydration shells in the cap waters (as are seen in bulk water), but in the channel this pattern is disrupted by the channel protein.

whereas the function for the cap water is asymptotic to 0, because of the finite size of the caps. For the channel water the secondary shells are smeared because of the inhomogeneous environment of waters due to the surrounding protein residues, resulting in a very different local environment for channel waters, as compared to bulk or cap waters, past the first solvation shell.

By suitably normalizing and integrating the pair correlation function of a given atom type with waters, we can calculate the average number of waters in a sphere of radius r around that atom type. The average number of waters within a distance corresponding to the first solvation shell yields the coordination number of water for that atom type. Applying this analysis to plots of oxygen-oxygen pair correlation function for water interacting with carboxyl, hydroxyl, and carbonyl oxygen (Fig. 4, *a*, *b*, and *c*, respectively), the coordination numbers of carboxyl, hydroxyl, and carbonyl oxygen with waters are found to be 3.5, 1, and 1, respectively. The coordination numbers extracted from the average number of hydrogen bonds between the water and various types of oxygen confirm these results. (Note that the correlation functions in Fig. 4, $n_{O\text{-}O'}$, are absolute rather than normalized to density, so that the integrals under the curves give the number of hydrogen bonds per oxygen atom.)

In Fig. 5 the total number of dihedral transitions during 312 ps of measurement cycle is shown for all 130 residues. The "dihedral transition" was defined as an event in which a side-chain dihedral angle moved from the vicinity of one dihedral relative energy minimum to the vicinity of another relative energy minimum. For example, suppose a particular dihedral angle has energy minima at 0°C, +120°C, and −120°C. Then a dihedral angle transition would be counted each time the trajectory of the dihedral angle versus time passed though +60°C, −60°C, or 180°C. The residues at the ends of the four helical segments of the channel undergo the largest number of transitions because they form fewer hydrogen bonds with other residues, and their motions are less coupled with those of other residues. Some of the hydrophobic residues, for example phenylalanine, which are on the outside of the modeled segment but not necessarily at the end of the segments, also show a large number of dihedral transitions. The hydrophilic residues near the narrow pore undergo relatively few dihedral transitions.

The water molecules in the narrowest part of the channel, near the turn section of the overall helix-turn-helix motif, had lower translational and orientational mobility than other waters and formed hydrogen bonds of unusually long duration with amino acids in that region. The overall translation of water through the channel was inhibited by these relatively restricted motions in the narrowest part of the channel. Some water molecules remained in the narrow part of the channel for the duration of the run. Others made a transition between other regions, where their motion was relatively freer, and the narrow part of the channel. Because only a few water molecules can be in this region at one time, the most revealing description of the motions of these

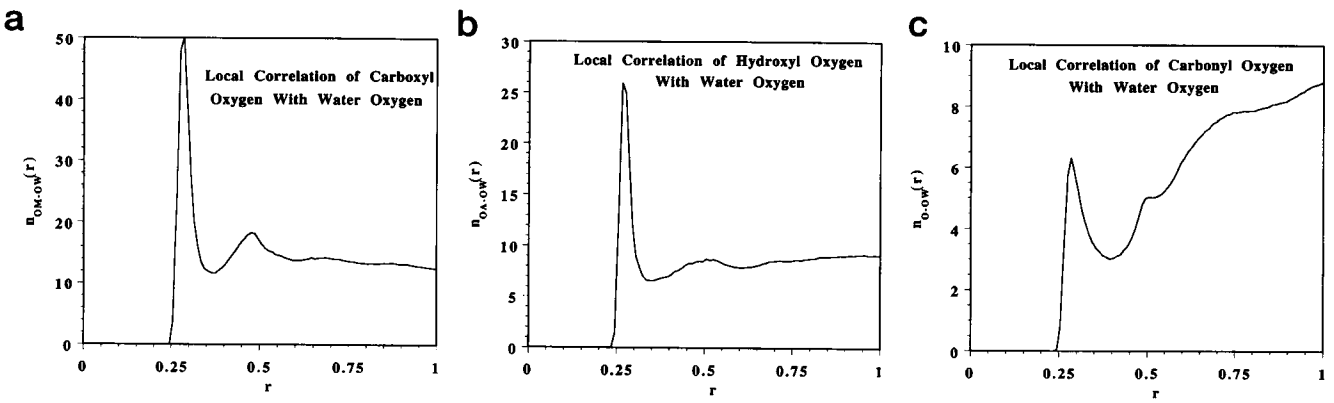

FIGURE 4 Oxygen-oxygen pair correlation function ($n_{O\text{-}O'}$) for water oxygens interacting with carboxyl (*a*), hydroxyl (*b*), and carbonyl (*c*) groups. The vertical axis is number density (hydrogen bonds per nanometer radial distance), and the horizontal axis is radial distance in nanometers. The pair correlation functions in this figure are not normalized for particle density. It can be seen that the coordination number is higher for interactions with the carboxyl than with the hydroxyl and carbonyl groups.

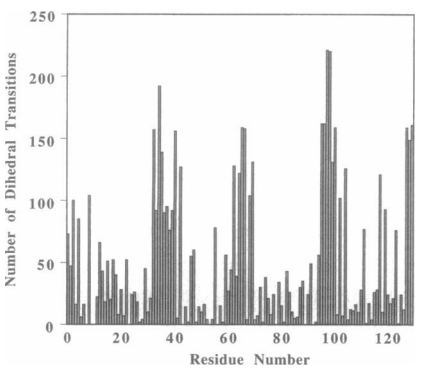

FIGURE 5 Histogram of number of dihedral angle transitions during the simulation for the various residues.

waters is singular rather than statistical. Thus, we plot in Fig. 6 *a–e* the z coordinate of the trajectories of several tagged waters, which spend a significant fraction of time near the narrow pore; their dipole moment orientation with the z axis; and the residue numbers (and names) of residues with which they form hydrogen bonds as a function of time. Note that the residue numbers are assigned in such a way that the residues with residue numbers not far away from each other are not necessarily close by in space. In comparing the different sections of Fig. 6, it will be seen that some water molecules are more stationary. These tend to be hydrogen bonded with particular residues near the narrow part of the channel. Others are more mobile during part of the molecular dynamics run. In Fig. 6 we show examples of both classes of water molecules.

In Fig. 6 *a* the z coordinate of one of the tagged waters shows that it starts out in one of the caps 19 Å away from the center of the channel. Within the next 50 ps it travels approximately 10 Å and enters the channel mouth. For the next 100 ps it moves back and forth in the channel, spanning an approximately 8-Å distance in both the forward and backward directions. However, for the latter half of the simulation the position of water appears to be very steady around $z = -2.5$ Å. In Fig. 6 *a* the dipole moment orientation (cos θ, where θ is the angle between the dipole moment of the water and the channel axis) of the same tagged water shows large and rapid changes in the orientation for the first 180 ps. Then for the latter part of the simulation the fluctuations are smaller. To understand the initial streaming and later steady motion and trends in the dipole moment orientation of the tagged water in terms of its hydrogen bond-forming patterns with various channel residues, we plot in Fig. 6 *a* the names and residue numbers of the residues that form hydrogen bonds with the tagged water. We find that during the first half of the simulations the tagged water does not form steady hydrogen bonds with any residue, and its hydrogen bond-forming partners change rapidly. At some instances the tagged water is hydrogen bonded only to other waters and not to any channel residues. These features are consistent with the large distance traveled by the water, which starts out in the cap and ends up in the channel close to the other cap. In the second half of the simulations the tagged water forms steady hydrogen bonds with 89 ASP and later with 56 GLU. It is because of these persistent hydrogen bonds that the water motion and its dipole moment orientation become steady.

The hydrogen bond patterns emerge from the concerted motion of the channel proteins and the tendency of the system to minimize its free energy by taking advantage of the new local potential energy minima created by the spatial rearrangements of the atoms. Based upon the fact that the motion of the channel protein sometimes favors large movements of water and propels the water into the channel mouth, we propose that a similar mechanism will account for the entry and movement of the ion into the channel.

In Fig. 6 *b* the z coordinate (coordinate along the channel axis) of another tagged water that spends all of the simulation time inside the channel is shown. This trajectory resembles discrete jumps between potential minima more than it does continuous diffusion. The corresponding dipole moment orientation also appears to be somewhat discretized.

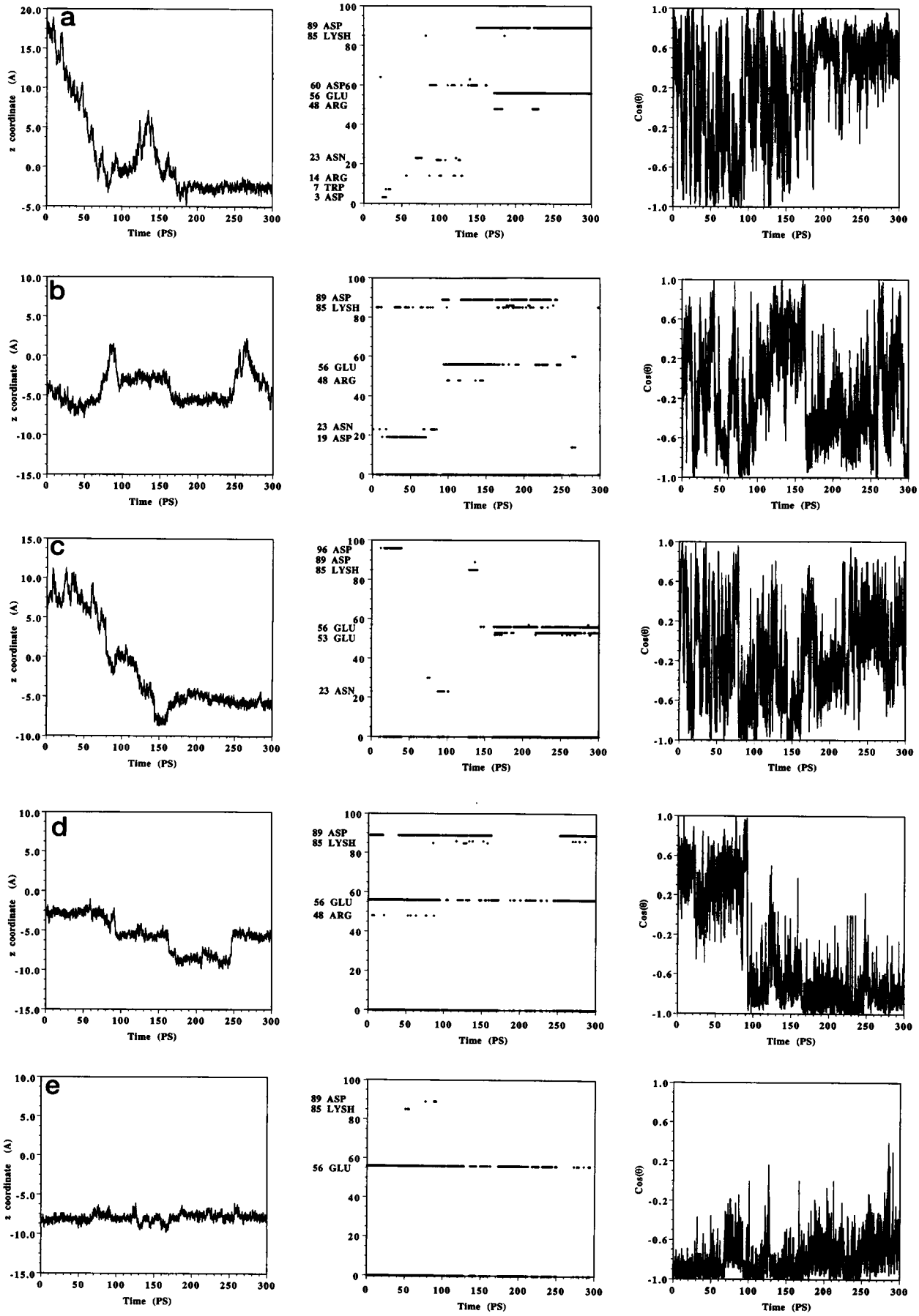
a
b
c
d
e
z coordinate (A)
Time (PS)
89 ASP
85 LYSH
60 ASP
56 GLU
48 ARG
23 ASN
14 ARG
7 TRP
3 ASP
19 ASP
96 ASP
53 GLU
Cos(θ)

To understand these trends we again investigate the hydrogen bond-forming patterns of the tagged water with the channel residues. It is seen that the relatively abrupt changes of position just before 100 ps, just after 150 ps, and after 250 ps each coincide with distinct changes in the protein-water hydrogen bonding pattern for that water molecule.

Fig. 6 *c* plots the *z* coordinate of a tagged water that starts out near one channel mouth and traverses 16 Å in 150 ps to get close to the other channel mouth. For the first 160 ps the water shows a large streaming motion, even though it is inside the channel and for the next 150 ps its motion is limited to distances on the order of 1 Å. From Fig. 6 *c* we can understand the above trends by noting the hydrogen bond-forming patterns of the tagged water. During the first 150 ps hydrogen bonds are formed with several residues for short periods of time, and for approximately 65 ps out of 150 ps only water-water hydrogen bonds are formed. For the next 150 ps hydrogen bonds with 56GLU and 53 GLU are present for a significant fraction of time, impeding the motion of water. The dipole moment orientation appears to be somewhat more localized in the second half of the simulation when the water mobility is low.

In Fig. 6 *d* we plot the *z* coordinate of a tagged water that spends all of the simulation time in the channel. The water traverses 6–7 Å inside the channel, but the traversal takes place in jumps, i.e., the *z* coordinate mostly remains steady, except during short periods of time when it suddenly switches to another value. The dipole moment orientation of the water appears to be rather localized, except for a distinct jump before 100 ps. As with other water molecules, the jumps in position (just before 100 ps, at about 170 ps, and at about 250 ps) correspond to distinct shifts in the protein-water hydrogen-bonding patterns.

In Fig. 6 *e* we plot the *z* coordinate and dipole moment orientation of a tagged water that remains in the channel and maintains a steady average *z* coordinate around −8 Å for the whole simulation. The dipole moment orientation of this water remains relatively localized. The hydrogen-bonding patterns of the tagged water in Fig. 6 *e* reveal that the above features are expected because it forms a steady hydrogen bond with 56 GLU for most of the simulation, except for rare hydrogen bonding with other residues and occasional formation of water-water hydrogen bonds.

In Fig. 7 *a* we plot the *z* coordinate of the center of mass of 19 waters that are inside the channel for the whole simulation period to detect any collective motion of the channel waters. We find that the center of mass of the water moves by only a few angstroms over the whole simulation time. Between 150 and 200 ps there appears to be a 2-Å jump in the *z* coordinate of the center of mass. By analyzing the *z* coordinate of the individual channel waters, we find

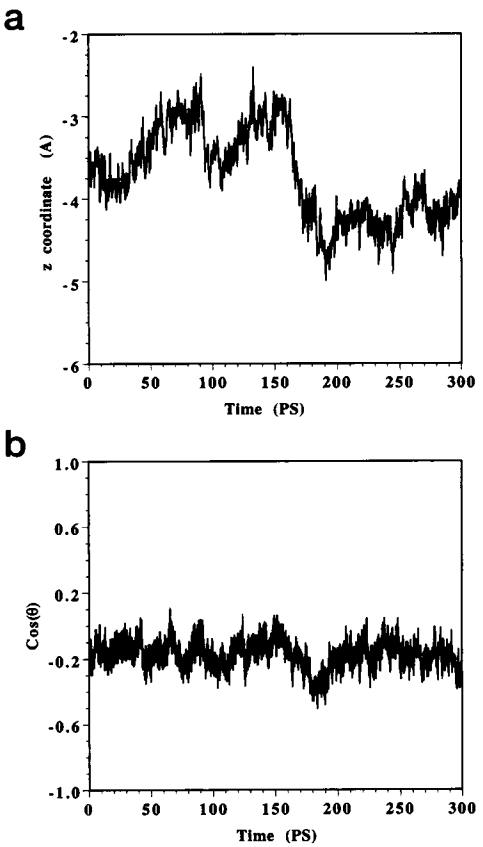

FIGURE 7 (*a*) Time course of the center of mass of the 19 water molecules that spent the entire simulation time inside the channel. (*b*) Time course of the mean cosine of the angle between the channel axis and the dipole moments of the 19 water molecules that spent the entire simulation time inside the channel.

that several waters undergo large movements during this period. The analysis of the hydrogen bond patterns shows that the large displacements of various channel waters are not associated with breaking hydrogen bonds with just a few residues. Rather different waters show jumps corresponding to a change in the hydrogen bonding pattern with different residues, and the apparent collective motion occurs because these events happen to occur at almost the same time. If simulations were performed for a longer period of time, there would be an occasional occurrence of such large collective motions.

In Fig. 7 *b* it is seen that the projection of the total dipole moment along the channel axis of the 19 waters that are always in the channel is nonzero. This net mean polarization of the channel water is apparently due to the asymmetrical shape of the channel and the inhomogeneous distribution of the hydrophilic residues. The direction of the net mean

FIGURE 6 This figure shows the nature of water movement by reference to five different individual water molecules (*a* through *e*). The projection of the trajectory along the channel axis (the *z* position), the normalized projection of the molecule's dipole moment along the channel axis, and the time course of the molecule's hydrogen bonding pattern with the channel protein are plotted for each molecule. Note that practically all of the long-lasting hydrogen bonds occur in or within a couple of residues of the hairpin turns in residues I, II, or III. These turns are segments 18–21, 52–55, and 84–87. In these figures $t = 0$ corresponds to the end of the 200-ps equilibration.

dipole moment is from the intracellular side to the extracellular side of the channel.

To distinguish the channel waters from the cap waters we plot in Fig. 8 the z coordinate and the dipole moment orientation of a tagged water that remains in the hemispherical cap during the whole simulation. The tagged cap water traverses an 18-Å distance in 150 ps, which is larger than the typical distance traversed by a channel water. The dipole moment orientation of the tagged cap water shows large and rapid fluctuations. The cap waters form hydrogen bonds mostly with other cap waters, except for a few that are within the hydrogen bond forming distance of the channel proteins. Because a smaller fraction of cap waters are within hydrogen bonding distance of the protein than is the case for channel waters, and because the water-water hydrogen bonds have shorter lifetimes than the water-protein hydrogen bonds, the cap waters have higher mobility.

To determine the fluid dynamic and the effective diffusion constant of channel and cap waters, we plot their mean square deviations in Fig. 9, *a* and *b*, respectively. The mean square deviations are separated into their x (solid line), y (dashed line), and z (dotted line) components, where Z is the

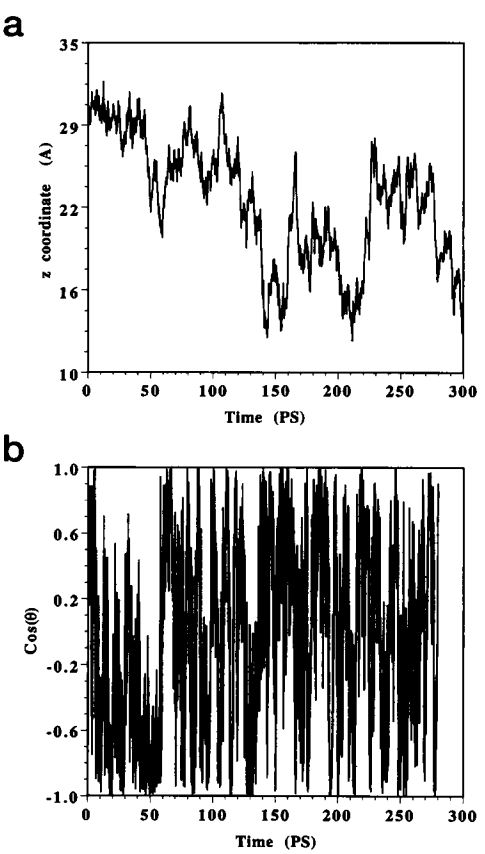

FIGURE 8 (*a*) Position along the z axis of a water molecule that spent its time in the cap. It is seen that the mobility is much higher than for a water molecule in the channel. (*b*) Time course of the cosine of the angle between the channel axis and the dipole moment of the cap water molecule in *a*. It is seen that the water in the cap has much more random rotational motion than water molecules in the channel (as seen in Fig. 6).

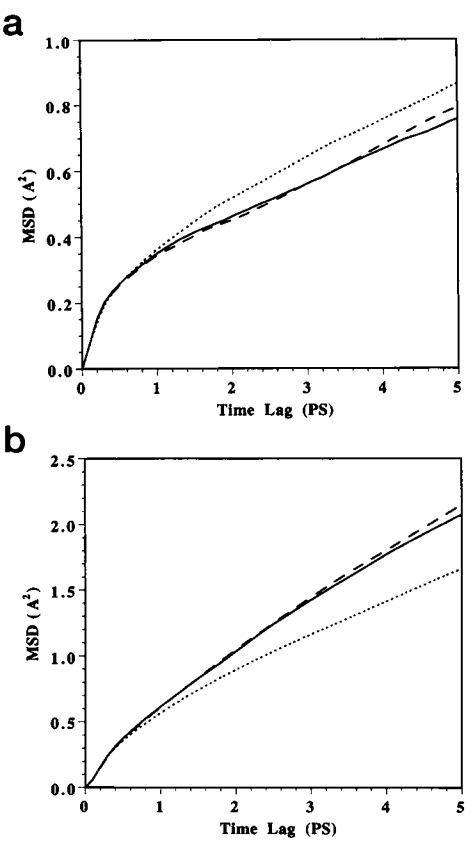

FIGURE 9 (*a*) Mean square deviation correlation function of the channel waters in each of the three spatial coordinates, x (——), y (– – –), and z (·····). The z dimension is the one along the channel axis. (*b*) Mean square deviation correlation function of the cap waters in each of the three coordinates (same coding of the dimensions as in *a*). It is seen that the cap waters have approximately bulk-like mobility, albeit with some anisotropy and restriction of motion associated with being restrained to the hemispherical caps. Comparison of *a* and *b* shows that being in the channel imposes a severalfold reduction in mobility on the water molecules.

dimension along the channel axis. These figures show that the effective diffusion constant of the channel water is higher along the channel axis than it is normal to the axis, presumably because of the confining effect of the channel structure. The effective diffusion coefficient of the cap water is slightly lower along the channel axis than it is normal to the axis. This anisotropy in the cap waters may be due to the boundary conditions that we impose to keep the water in the cap, but it is small enough that we do not feel that our essential assumption that the cap water is bulk-like is seriously compromised. The approximate hydrodynamic diffusion constants of the channel and cap waters are 0.375 and 0.55 Å^2/ps, respectively, and the effective diffusion constants are 0.05 and 0.19 Å^2/ps, respectively. The hydrodynamic diffusion constant of cap water is comparable to that of bulk SPC water, i.e., about 0.6 Å^2/ps. The effective diffusion coefficient is smaller than that in our simulation because of the relatively small size of the water cap. However, we believe that the local behavior of the cap water is bulk-like. One reason is that the peaks in the oxygen-oxygen

radial distribution function for the cap water (Fig. 3 *b*) have essentially the same position and width as the corresponding peaks for a bulk simulation of SPC water (Chiu, personal communication). Morover, in a previous study on gramicidin we used the same methods but an even smaller cap, and found that the spectral properties of the cap water (the velocity autocorrelation function and its spectral density function) were essentially identical to those of bulk water (Chiu et al., 1991).

The mean square deviation of the center of mass of 19 channel waters in Fig. 10 *a* shows that the hydrodynamic and effective diffusion constants for the center of mass are 0.035 and 0.007 Å^2/ps, respectively, both of which are an order of magnitude smaller than that for individual channel waters. This result is quite different from the corresponding result in gramicidin channels (Chiu et al., 1991, 1993), in which the effective diffusion coefficient for the center of mass of channel waters is the same as for individual waters. The difference shows that in the sodium channel it is quite common for water molecules to move past each other in translocation through the channel, as opposed to gramicidin channels, in which the column of waters move in obligatory single file. To investigate whether the fluctuations in the protein structure play a key role in steering the water through the channel, we also calculate the MSD and diffusion constants for a system with frozen protein structure. The freezing of the protein conformation is achieved by keeping it at 3°K while the water temperature remains at 300°K. In Fig. 10 *b* we plot the MSD of the channel waters with frozen protein structure, which shows that both the hydrodynamic and effective diffusion constants of the channel water are very small (0.12 and 0.004 Å^2/ps, respectively). This leads us to conclude that the fluctuations in the protein structures are vital for the motion of water through the channel.

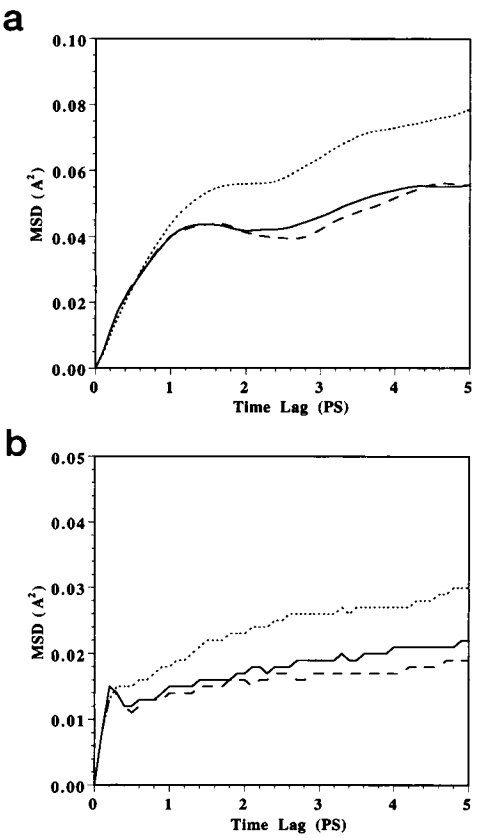

FIGURE 10 (*a*) Mean square deviation of the center of mass of the 19 waters that are always in the channel (same set as Fig. 9 *a*). The *x*, *y*, and *z* directions are the solid, dashed, and dotted curves respectively. The *z* dimension is the one along the channel axis. Comparing Fig. 9 *a* to *a* shows that the effective diffusion coefficient of the center of mass is much less than for the individual channel waters. This implies that the water molecules can move past each other in the channel as opposed to single-filing and permeating as a unit, as in the gramicidin channel. (*b*) Mean square deviation of individual channel waters for the simulation in which the protein is frozen to 3°K while the water temperature remains at the normal 300°K. In comparing *b* with Fig. 9 *a* it is seen that freezing the protein dramatically reduces the water mobility, showing that fluctuations in the protein structure are vital for the motion of water through the channel.

Analysis of the interaction energy between the ion and different channel residues indicates that the interaction energy is stronger for the LYS 85 than for any other single residue (see Table 1). This energy is unfavorable for the positive ions and favorable for the chloride ions. However, this effect is more than outweighed by the sum of the interactions with other nearby negative residues such as ASP 19, GLU 53, GLU 56, ASP 89, and ASP 120, so that the net effect of the charge distribution in the narrowest part of the pore is to favor cations over anions (Table 1).

DISCUSSION AND SUMMARY

This paper has described the solvation of a putative model for the selectivity filter and part of the pore region of a sodium channel. The model was produced by Guy and Durell (1995). It is not clear how correct this model is, but it seems very likely that it has some significant features in common with the correct model. It comprises the P region, which is implicated as the pore and selectivity filter by electrophysiology and mutagenesis studies. The structure is oriented in such a way that the majority of charged residues are oriented toward the aqueous lumen of the channel. The narrowest portion of the structure is quite short, consistent with the flux ratio data that imply that only one sodium ion at a time normally occupies the narrowest portion of the channel.

The solvation and water transport properties of the sodium channel were compared with corresponding properties of the gramicidin channel, as they had been determined in previous studies (Chiu et al., 1989, 1991, 1992, 1993). The properties were different from gramicidin in one significant way and similar in other ways. The major difference was that in the sodium channel model the waters do not move in obligatory single file, whereas in the gramicidin channel they do. The evidence for this statement lies in the finding that in gramicidin the effective diffusion coefficient of the center of mass of the channel water is the same as the

effective diffusion coefficient of the individual waters, whereas in the sodium channel the effective diffusion coefficient of the center of mass of all of the channel waters is much less than that of the individual channel waters. For the sodium channel the relevant effective diffusion coefficient for describing net transport through the channel is that for the individual water molecules in the channel rather than the center-of-mass diffusion coefficient.

The polarization of water in the gramicidin and the sodium channels is somewhat different. In the gramicidin channel we found a strong tendency for all the water molecules in the channel to have their dipole moments facing in approximately the same direction at any instant (Chiu et al., 1989, 1991, 1996a). Averaged over a long time the mean dipole moment of the waters in the gramicidin channel is zero, because of periodic collective shifts in the polarization of the entire water chain. Within the sodium channel, by contrast, there is a much greater variation in the distribution of dipole moment vectors at any moment. However, it appears from our data that the mean dipole moment of the waters in the channel averaged over a long time is nonzero, in response to the P-region of the channel itself having a net nonzero polarization.

In other ways the solvation and transport of water in the sodium channel are similar to that in the gramicidin channel. In both channels the effective diffusion coefficient governing water transport in the channel is several times smaller than the water diffusion coefficient in bulk. In both channels water motion depends on protein motion, as shown by the fact that if the protein is immobilized by extreme temperature reduction, the water is also effectively immobilized, even if kept at 300°K. The basis for the dependence on protein motion in both cases is that the water mobility strongly depends on the lifetime of water-protein hydrogen bonds. However, there are interesting differences in the precise nature of the protein-water hydrogen bonding in the two systems. In gramicidin a large majority of the waters at any instant are hydrogen bound to the protein. In the sodium channel, because the channel is wider, only a minority of the waters in the channel are hydrogen bound to the protein at any one time. Thus it was not obvious to us before doing the calculation that immobilizing the protein would immobilize the channel waters as completely as it did. Another difference in the nature of the protein-water hydrogen bonding is that in gramicidin the hydrogen bonding is to the protein backbone, whereas in the sodium channel it is to charged atoms in the side chains. In the gramicidin channel practically all of the protein-water hydrogen bonds are between water hydrogens and carbonyl oxygens. In the sodium channel there is a more equal distribution of the polarity of the bonds. Significant numbers of bonds are made between water oxygens and positive atoms in the sodium channel protein and between water hydrogens and negative atoms in the sodium channel protein. The relative immobilization of the hydrogen-bonded waters in the narrow part of the channel seems similar to that seen in water clusters around charged groups on the surface of a partially hydrated globular protein (Steinbach and Brooks, 1993).

For all of the differences in the details of hydrogen bonding, the major similarities hold that water in both the gramicidin and the sodium channel has a severalfold reduced mobility compared to bulk water, and the mobility in the channel is strongly dependent on protein motion. The reduction of water mobility in our simulated channel provides support for a possible explanation for the experimentally observed reduction of mobility of polyethylene glycols of various sizes in alamethicin channels (Bezrukov et al., 1994). Because the mobility of the polymers in the channel does not vary significantly with polymer size, it seems likely that the reason for the reduced mobility of the polymer is the reduced mobility of the water, as we see in our simulations.

An interesting question is, how dependent on the specific model used are solvation properties of the channel? In particular, would similar results be obtained from the β-hairpin model of Lipkind and Fozzard (1994)? This cannot be determined without doing the explicit calculations. Somewhat relevant results are given by Sansom et al. (1996). In these studies water mobilities and orientations are studied in model pores whose walls consist of α-helices and β-strands. It is found in each case that water translational and orientational mobility is substantially reduced from bulk. In the one case in which the channel has a polarization along its length (parallel α-helices), there is a net preference for water dipoles to line up counter to the helix dipole. These results suggest the possibility that one might be able to generalize that water in channels will be reduced in mobility and will orient with respect to the polarity of the channel protein, but further investigations are needed to establish the extent of this generalizability.

Studies of ion selectivity by energy minimization (Table 1) show clearly the basis for the putative channel structure to select for cations over anions. The energy minimization method is not powerful enough to suggest any basis for sodium over potassium selectivity, because it does not comprehensively sample configurations of the protein, water, and ions along the ionic permeation pathway. Future work will involve potential-of-mean force computations in which molecular dynamics is done with ions restrained in the vicinity of various positions along the permeation pathway (as in, for example, Roux and Karplus, 1993). In addition to configuration sampling, a second concern is whether the sodium/potassium selectivity depends critically on the width of the channel in the narrowest region. Some evidence for this lies in experiments that show a difference between potassium and sodium channels in the size of the largest ions that can pass throught the selectivity filter (Hille, 1992). Thus future calculations should include adjusting spacing between the subunits to test the effects of minimum channel size on sodium/potassium selectivity.

We gratefully acknowledge H. Robert Guy for supplying the initial coordinate file for the sodium channel pore model. See-Wing Chiu provided

helpful advice and analysis programs, and shared with us his computed data for the bulk water radial distribution function (used in Fig. 3) and his computed structure for the gramicidin channel in a lipid bilayer (used in Fig. 1 *e*). Oliver Smart shared his program HOLE for us to calculate the channel radius (Fig. 1 *e*). Dr. Adrian Parsegian drew our attention to the possible connection between our computations and the experimental work of Bezrukov et al.

This work was supported by a grant from the National Science Foundation. Simulations were done at the National Center for Supercomputing Applications located in the Beckman Institute for Advanced Science and Technology, Urbana, Illinois.

REFERENCES

Aqvist, J. 1990. Ion-water interaction potentials derived from free energy perturbation methods. *J. Phys. Chem.* 94:8021–8024.

Arseniev, A. S., I. L. Barsukov, V. F. Bystrov, A. L. Lomize, and Yu. A. Ovchinnikov. 1985. ^{1}H-NMR study of gramicidin A transmembrane channel. Head-to-head right-handed, single-stranded helices. *FEBS Lett.* 186:168–174.

Berendsen, H. J. C., J. P. M. Postma, W. F. van Gunsteren, A. DiNola, and J. R. Haak. 1984. Molecular dynamics with coupling to an external bath. *J. Chem. Phys.* 81:3684–3689.

Bezrukov, S. M., I. Vodyanoy, and V. A. Parsegian. 1994. Counting polymers moving through a single ion channel. *Nature.* 370:279–281.

Chiu, S. W., K. Gulukota, and E. Jakobsson. 1992. Computational approaches to understanding the ion channel-lipid system. *In* Membrane Proteins: Structures, Interactions, and Models. A. Pullman, B. Pullman, and J. Jortner, editors. Kluwer, Amsterdam, The Netherlands.

Chiu, S.-W., E. Jakobsson, S. Subramaniam, and J. A. McCammon. 1991. Time-correlation analysis of simulated water motion in flexible and rigid gramicidin channels. *Biophys. J.* 60:273–285.

Chiu, S. W., J. A. Novotny, and E. Jakobsson. 1993. The nature of ion and water barrier crossing in a simulated ion channel. *Biophys. J.* 64:98–108.

Chiu, S. W., S. Subramaniam, and E. Jakobsson. 1996a. Simulation of a gramicidin channel in a fluid phase DMPC bilayer. *Biophys. J.* 70:A80.

Chiu, S. W., S. Subramaniam, and E. Jakobsson. 1996b. Simulation of a fully hydrated DMPC bilayer using the NγT boundary conditions. *Biophys. J.* 70:A94.

Chiu, S-W., S. Subramaniam, E. Jakobsson, and J. A. McCammon. 1989. Water and polypeptide conformations in gramicidin channels—a molecular dynamics study. *Biophys. J.* 56:253–261.

Favre, I., E. Moczydlowski, and L. Schild. 1996. Structural determinants for K^+ and Ca^{2+} selectivity in the voltage-gated Na channel. *Biophys. J.* 70:A78.

Guy, H. R., and S. R. Durell. 1995. Structural models of Na^+, Ca^{2+}, and K^+ channels. *In* Ion Channels and Genetic Diseases. D. C. Dawson and R. A. Frizzell, editors. Rockefeller University Press, New York.

Guy, H. R., and P. Seetharamulu. 1986. Molecular model of the action potential sodium channel. *Proc. Natl. Acad. Sci. USA.* 83:508–512.

Heinemann, S. H., H. Terlau, Stühmer, K. Imoto, and S. Numa. 1992. Calcium channel characteristics conferred on the sodium channel by single mutations. *Nature.* 356:441–443.

Hermans, J., H. J. C. Berendsen, W. F. van Gunsteren, and J. P. M. Postma. 1984. A consistent empirical potential for water-protein interactions. *Biopolymers.* 23:1513–1518.

Hille, B. 1992. Ionic Channels of Excitable Membranes, 2nd Ed. Sinauer Associates, Sunderland, MA.

Kim, M.-K., T. Morii, L.-X. Sun, K. Imoto, and Y. Mori. 1993. Structural determinants of ion selectivity in brain calcium channel. *FEBS Lett.* 318:145–148.

Lipkind, G. M., and H. A. Fozzard. 1994. A structural model of the tetrodotoxin and saxitoxin binding site of the Na^+ channel. *Biophys. J.* 66:1–13.

Mikala, G. A., A. Bahinski, A. Yatani, S. Tang, and A. Schwartz. 1994. Differential contribution by conserved glutamate residues to an ion-selectivity site in the L-type Ca^{2+} channel pore. *FEBS Lett.* 335: 265–269.

Nicholson, L. K., and T. A. Cross. 1989. The gramicidin channel: an experimental determination of the right-handed helix sense and verification of β-type hydrogen bonding. *Biochemistry.* 28:9379–9385.

Roux, B., and M. Karplus. 1993. Ion transport in the gramicidin channel: free energy of the solvated right-handed dimer in a model membrane. *J. Am. Chem. Soc.* 115:3250–3260.

Sansom, M. S. P., I. D. Kerr, J. Breed, and R. Sanararamakrishnan. 1996. Water in channel-like cavities: structure and dynamics. *Biophys. J.* 70:639–702

Smart, O. S., J. M. Goodfellow, and B. A. Wallace. 1993. The pore dimensions of gramicidin A. *Biophys. J.* 65:2455–2460.

Steinbach, P. J., and B. R. Brooks. 1993. Protein hydration elucidated by molecular dynamics simulation. *Proc. Natl. Acad. Sci. USA.* 90: 9135–9139.

Terlau, H., S. H. Heinemman, W. Stühmer, M. Pusch, F. Conti, H. Imoto, and S. Numa. 1991. Mapping the site of tetrodotoxin and saxitoxin of sodium channel II. *FEBS Lett.* 293:93–96.

Urry, D. W. 1971. The gramicidin A transmembrane channel: a proposed $\pi_{(L,\,D)}$ helix. *Proc. Natl. Acad. Sci. USA.* 68:672–676.

White, S. H., editor. 1994. Membrane Protein Structure: Experimental Approaches. Oxford University Press, New York.

Yang, J., P. T. Ellinor, W. A. Sather, J.-F. Zhang, and R. W. Tsien. 1993. Molecular determinants of Ca^{2+} selectivity and ion permeation in L-type Ca^{2+} channels. *Nature.* 366:158–161.